

Spatially tunable spin interactions in neutral atom arrays

Lea-Marina Steinert,^{1,2,3,*} Philip Osterholz,^{1,2,3} Robin Eberhard,^{1,2} Lorenzo Festa,^{1,2}
 Nikolaus Lorenz,^{1,2} Zaijun Chen,^{1,2} Arno Trautmann,^{1,2,3} and Christian Gross^{1,2,3}

¹*Max-Planck-Institut für Quantenoptik, 85748 Garching, Germany*

²*Munich Center for Quantum Science and Technology (MCQST), 80799 München, Germany*

³*Physikalisches Institut, Eberhard Karls Universität Tübingen, 72076 Tübingen, Germany*

(Dated: November 7, 2022)

Analog quantum simulations with Rydberg atoms in optical tweezers routinely address strongly correlated many-body problems due to the hardware-efficient implementation of the Hamiltonian. Yet, their generality is limited, and flexible Hamiltonian-design techniques are needed to widen the scope of these simulators. Here we report on the realization of spatially tunable interactions for XYZ models implemented by two-color near-resonant coupling to Rydberg pair states. Our results demonstrate the unique opportunities of Rydberg dressing for Hamiltonian design in analog quantum simulators.

Quantum simulators based on arrays of neutral atoms have proven to be among the most promising platforms to address non-trivial problems of strongly correlated many-body phenomena. This success is based on the optimally hardware-efficient analog implementation of the Hamiltonian under study [1–4], which is one of the reasons to employ these machines for useful tasks in the so-called NISQ (noisy intermediate-scale quantum) era of quantum processors. While such an emulation approach eliminates any overhead in control necessities or qubit numbers, it strongly restricts the use cases of a specific quantum simulator to problems rooted in the device-dependent Hamiltonian. Here, neutral atoms trapped in optical tweezer arrays with engineered geometries in two dimensions, laser coupled to Rydberg states to induce interactions [5], are among the most promising platforms [6–12]. Large system sizes have been demonstrated with long coherence times [12, 13], enabling the simulation of quantum magnets both in equilibrium [14, 15] and dynamically [16].

Rydberg atom-based simulators naturally implement Ising or XY-type Hamiltonians with power-law interactions [17–20]. Recently, Floquet-engineered XXZ spin coupling in bulk systems and optical tweezer arrays has been demonstrated [21, 22]. Control over the spatial interaction profile of Ising systems has also been realized by admixing Rydberg character to the ground state, so-called Rydberg dressing [23–30]. Lately, a sharply peaked interaction profile has been demonstrated by coupling to molecular Rydberg macrodimer potentials [31]. One of the biggest remaining challenges is to increase the systems’ flexibility via universally programmable analog qubit couplings.

We report on progress into this direction by the realization of freely tunable short-range XYZ-type spin interactions between atoms trapped in optical tweezer arrays. The effective spin-1/2 system is encoded in two electronic ground states and we introduce interactions by two-color Rydberg dressing. This allows to engineer the

spin-spin couplings in each spin direction by the choice of the laser parameters. Our approach uses the spatially dependent van-der-Waals (vdW) interactions between different m_j -sublevels in the Rydberg pair state manifold to design distance and angular-dependent couplings of the XYZ Hamiltonian [33]

$$\hat{H}_{\text{XYZ}} = \hbar \sum_{i < j} (J_{ij}^z \hat{\sigma}_i^z \hat{\sigma}_j^z + J_{ij}^{++} \hat{\sigma}_i^+ \hat{\sigma}_j^+ + J_{ij}^{+-} \hat{\sigma}_i^+ \hat{\sigma}_j^-) + h.c. \quad (1)$$

The Pauli matrices $\hat{\sigma}_j^z$, $\hat{\sigma}_j^x = (\hat{\sigma}_j^+ + \hat{\sigma}_j^-)$ and $\hat{\sigma}_j^y = i(\hat{\sigma}_j^- - \hat{\sigma}_j^+)$ describe a spin-1/2 particle at position j . This Hamiltonian distinguishes between three types of spin couplings J_{ij}^γ : The diagonal interaction between dressed ground states J_{ij}^z , the off-diagonal “flop-flop” J_{ij}^{++} , and “flip-flop” J_{ij}^{+-} interactions. While dressing-induced Ising (J^z) interactions have already been studied in various experiments [26, 27, 30, 31, 34–36] and programmable long-range interactions have been demonstrated in optical cavities [37], we focus on programmable J_{ij}^{++} and J_{ij}^{+-} interactions (see fig. 1). With control over the laser parameters and the geometric arrangement of single atoms, we can engineer the relative coupling strength of the spin-spin interactions J_{ij}^{++}/J_{ij}^z and J_{ij}^{+-}/J_{ij}^z as visualized exemplarily in fig. 2. We are also able to switch off specific couplings globally by the choice of the laser detunings as discussed below. In a 2D configuration, the situation is even more complex: The angular dependence of the interaction provides a unique opportunity to control the nearest-neighbor- versus longer-ranged interaction and to realize models featuring various magnetic phenomena, including frustration and topology [7, 10, 33, 38–40]. Our approach also opens new pathways to quantum simulations with practical relevance for the inference of Hamiltonians underlying spectra obtained in nuclear magnetic resonance experiments in chemistry and biology [41].

The physical system we use is an optical tweezer array of single ³⁹K atoms. The spins are encoded in the

* lea.steinert@uni-tuebingen.de

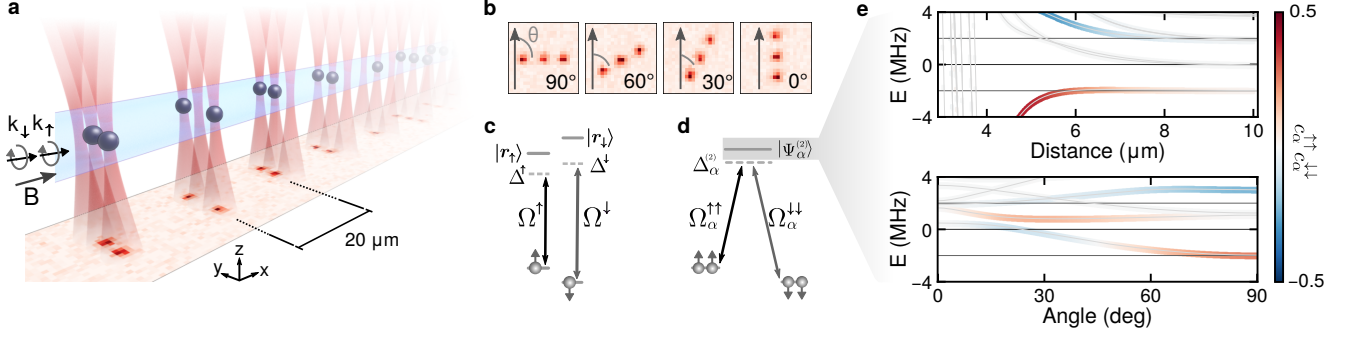


Figure 1. **Experimental setup and level schemes.** **a.** Illustration of the experimental setting. The Rydberg excitation beams (\mathbf{k}_\uparrow and \mathbf{k}_\downarrow , light blue) are aligned along the magnetic field \mathbf{B} , driving σ^- transitions. They illuminate all tweezer groups, each with three linearly arranged tweezers (red), which are statistically loaded with atoms (black spheres). At the bottom of the illustration, a single shot fluorescence image is shown. **b.** Example of fluorescence images of fully loaded tweezer groups for various angles θ at a distance of $5.2 \mu\text{m}$. **c.** On the single-atom level, we couple the electronic ground states $|\uparrow\rangle$ and $|\downarrow\rangle$ to the Rydberg states $|r_\uparrow\rangle$ and $|r_\downarrow\rangle$ with Rabi frequencies ($\Omega^\uparrow, \Omega^\downarrow$) and detunings ($\Delta^\uparrow, \Delta^\downarrow$). **d.** Schematic for the flop-flop interaction J_{ij}^{++} between two atoms i and j . Via adiabatic elimination of the singly excited pair states, we reduce the four-photon process to an effective Λ -scheme. The pairs of ground state atoms are coupled with the effective Rabi couplings $\Omega_\alpha^{\uparrow\uparrow}$ and $\Omega_\alpha^{\downarrow\downarrow}$ to Rydberg pair states $|\Psi_\alpha^{(2)}\rangle$. $\Delta_\alpha^{(2)}$ is the two-photon detuning to each $|\Psi_\alpha^{(2)}\rangle$, which includes interaction induced shifts. **e.** Calculated eigenenergies of \hat{H}_{Ryd} depending on the atom pair distance d at an angle of $\theta = 90^\circ$ (upper) and atom pair angle θ at a distance $d = 6 \mu\text{m}$ (lower). The color scale corresponds to the overlap $c_\alpha^{\uparrow\uparrow} c_\alpha^{\downarrow\downarrow}$. The solid lines at $\pm 2 \text{ MHz}$ mark the energy of the asymptotic Rydberg pair state $|r_\downarrow r_\downarrow\rangle$ and $|r_\uparrow r_\uparrow\rangle$. The theoretical results are obtained by exact diagonalization of H_{Ryd} using the “pairinteraction” software package [32].

hyperfine states $|\uparrow\rangle = |4S_{1/2} F = 2, m_F = -2\rangle$ and $|\downarrow\rangle = |4S_{1/2} F = 1, m_F = -1\rangle$. Both states are coupled individually to the Rydberg states $|r_\uparrow\rangle = |62P_{3/2}, m_j = -3/2\rangle$ and $|r_\downarrow\rangle = |62P_{3/2}, m_j = -1/2\rangle$ by off-resonant single photon excitation at 286 nm with the Rabi frequencies Ω^\uparrow and Ω^\downarrow , and detunings Δ^\uparrow and Δ^\downarrow (see Fig. 1). The choice of beam polarizations suppresses single-atom Raman couplings. In this doubly laser-coupled system, rich spin-spin interactions emerge, which are rooted in the strong van der Waals (vdW) interactions between the addressed Rydberg pair states. For the derivation of the spin couplings J_{ij}^{++} and J_{ij}^{+-} , we start with diagonalizing $\hat{H}_{\text{Ryd}} = \hat{H}_{\text{las}} + \hat{H}_{\text{int}}$ in the Rydberg pair state basis [33]. Here, \hat{H}_{las} is the single atom Hamiltonian in the rotating frame. The vdW Hamiltonian \hat{H}_{int} leads to interactions between the different m_j levels in the $62P_{3/2}$ manifold. We admix different components of the vdW pair eigenstates to the ground states by laser coupling to obtain the effective interactions between the ground states.

The interactions in Eq. 1 can be understood as four-photon processes by adiabatic elimination of all excited states (Supplementary Information and ref. [33]). For example, for the flop-flop interactions, the coupling of the $|\uparrow\uparrow\rangle$ pair ground state to a Rydberg pair eigenstate $|\Psi_\alpha^{(2)}\rangle$ follows by adiabatic elimination of the singly excited state as $\Omega_\alpha^{\uparrow\uparrow} = (\Omega^\uparrow)^2 \cdot c_\alpha^{\uparrow\uparrow} / 2\Delta^\uparrow$, where $c_\alpha^{\uparrow\uparrow} = \langle \Psi_\alpha^{(2)} | r_\uparrow r_\uparrow \rangle$ is the wavefunction overlap of one eigenstate $|\Psi_\alpha^{(2)}\rangle$ in the Rydberg manifold with the asymptotic Ry-

berg pair state $|r_\uparrow r_\uparrow\rangle$. The coupling of $|\downarrow\downarrow\rangle$ follows analogously. For sufficiently large detuning of the lasers to any coupled state in the Rydberg manifold, we can furthermore eliminate the Rydberg pair eigenstates to arrive at an effective coupling between ground state atom pairs i and j :

$$J_{ij}^{++} = 2 \sum_\alpha \frac{\Omega_\alpha^{\uparrow\uparrow} \Omega_\alpha^{\downarrow\downarrow}}{\Delta_\alpha^{(2)}} = \frac{(\Omega^\uparrow \Omega^\downarrow)^2}{4\Delta^\uparrow \Delta^\downarrow} \cdot \frac{c_\alpha^{\uparrow\uparrow} c_\alpha^{\downarrow\downarrow}}{\Delta_\alpha^{(2)}} \quad (2)$$

The Rydberg pair state detuning $\Delta_\alpha^{(2)}$ includes vdW interaction-induced shifts $U_{\text{vdW},\alpha}$. Spin flips from $|\uparrow\uparrow\rangle$ to $|\downarrow\downarrow\rangle$ and vice versa require a non-zero probability overlap $c_\alpha^{\uparrow\uparrow} c_\alpha^{\downarrow\downarrow}$ provided by the mixing of the m_j -sublevels.

The derivation of J_{ij}^{+-} starts with two atoms in opposite spin states $|\uparrow\downarrow\rangle$ or $|\downarrow\uparrow\rangle$. Different from the flop-flop interaction case, there are two excitation paths to the Rydberg manifold. Via adiabatic elimination of the intermediate singly excited state we obtain an effective two-photon coupling $\Omega_\alpha^{\uparrow\downarrow} = \Omega^\uparrow \Omega^\downarrow \cdot c_\alpha^{\uparrow\downarrow} \cdot (1/4\Delta^\uparrow + 1/4\Delta^\downarrow)$. Then, in fourth order perturbation theory, we obtain the flip-flop interaction:

$$J_{ij}^{+-} = 2 \sum_\alpha \frac{\Omega_\alpha^{\uparrow\downarrow} \Omega_\alpha^{\downarrow\uparrow}}{\Delta_\alpha^{(2)}} = \sum_\alpha \frac{(\Omega^\uparrow \Omega^\downarrow)^2}{16(\Delta^\uparrow \Delta^\downarrow)^2} \cdot (\Delta^\uparrow + \Delta^\downarrow)^2 \cdot \frac{c_\alpha^{\uparrow\downarrow} c_\alpha^{\downarrow\uparrow}}{\Delta_\alpha^{(2)}} \quad (3)$$

For finite flip-flop interaction, we require a non-zero overlap of $c_\alpha^{\uparrow\downarrow} c_\alpha^{\downarrow\uparrow}$. In the case of symmetric detunings

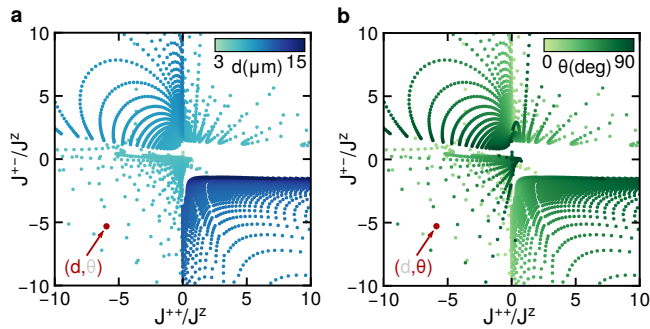


Figure 2. **Tunable XYZ interactions in 1D chains.** In both panels we show the calculation of the same data points, highlighting the distance **(a.)** and angle **(b.)** dependence of the ratios J_{ij}^{++}/J_{ij}^z and J_{ij}^{+-}/J_{ij}^z for one exemplary set of detunings $(\Delta^\uparrow, \Delta^\downarrow) = 2\pi \cdot (1.4, -0.6)$ MHz. The interactions are calculated for distances spaced by 100 nm and angles in steps of 1° . Quadrant II and IV show a smooth tunability, while the ratios in quadrant I and III are realized close to Rydberg pair state resonances. The latter requires higher stability of the control parameters, but may ultimately be beneficial for the achievable coherence [38].

$\Delta^\uparrow = -\Delta^\downarrow$, the flip-flop interaction is generally canceled by destructive interference of the excitation paths. This provides us with sensitive control of J_{ij}^{+-} by choosing the excitation laser detuning accordingly. In contrast, energy conservation restricts the flop-flop processes and requires the laser detunings to be set to $\Delta^\uparrow - \Delta^\downarrow = E_z$, with E_z the Zeeman splitting between $|r^\uparrow\rangle$ and $|r^\downarrow\rangle$ (see Fig. 3c).

To study the dependence of the interaction strengths on the geometric arrangement experimentally, we select the simplest possible setting of three in-line traps with various nearest-neighbor (nn) distances d and angles θ (see Fig. 1a,b). Here, θ is the angle between the interatomic separation vector \mathbf{d} and the magnetic field \mathbf{B} , which is set to 1 G and defines the quantization axis. We use 14 replications of this pattern for increased statistics, where the inter-group spacing is $20 \mu\text{m}$, larger than any interaction range in the system. With a first fluorescence image of the atom array, we check for the presence of an atom in the trap. We then prepare all atoms in the $|\uparrow\rangle$ state and perform Raman sideband cooling. This allows us to minimize the trap induced inhomogeneities by working at the lowest possible tweezer depth of $h \cdot 80 \text{kHz}$ [42] (Supplementary Information). We then apply two-color Rydberg dressing for $50 \mu\text{s}$. Next, we remove all $|\uparrow\rangle$ atoms by a blowout pulse and detect only the remaining atoms in the $|\downarrow\rangle$ state with a second fluorescence image. Comparing both fluorescence images allows us to infer the spin interactions by observing flipped spins and their correlations.

First, we aim to reveal the induced flop-flop interactions by choosing our detuning symmetric $\Delta^\uparrow = -\Delta^\downarrow$,

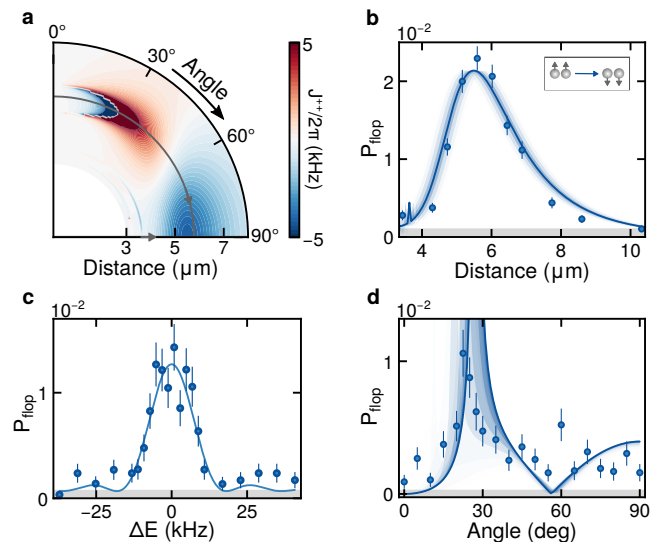


Figure 3. **Flop-flop interactions.** **a.** Calculation of J^{++} as a function of θ and d for $\Delta_\uparrow = -\Delta_\downarrow = 2\pi \cdot 1$ MHz. We identify a resonance in the spin-spin couplings appearing as a singularity around $\theta = 30^\circ$ at a distance of $5 - 6 \mu\text{m}$. **b.** Observed flop-flop probability P_{flop} for different atom pair distances at $\theta = 90^\circ$. A small false positive probability sets the detection limit (grey area) taking into account single spin flips and inefficient state preparation and push out. Error bars indicate 1 s.e.m. The solid line corresponds to the theoretical prediction, where the amplitude has been scaled to match the experimental values due to broadening effects. The blue shading indicates the effect of the finite radial size of the atomic wavepacket σ_{rad} (Supplementary Information). Each shading represents the interaction difference for $\sigma_{\text{rad}}/2$ steps in pair distance in the range of $\pm 3\sigma_{\text{rad}}$. **c.** Flop-flop processes versus two-atom Raman detuning $\Delta E = E_z - \Delta^\uparrow + \Delta^\downarrow$. The fit shows the characteristic sinc² envelope of a Fourier limited rectangular pulse with a full width half maximum $\text{FWHM} = (18.2 \pm 0.2) \text{kHz}$. **d.** Angular dependence of the flop-flop interaction at a distance of $5.6 \mu\text{m}$.

to cancel the flip-flop terms. We map the spatial dependence of the interactions by preparing the atoms at different distances and angles. We do not observe significant single spin flips, confirming the suppression of single-atom Raman processes. The J^{++} interaction leads to pairwise spin-flips, which we observe in our setting between nearest neighbors. The distance dependence of the pairwise spin flips is shown in Fig. 3, where we scan the atoms' distances at $\theta = 90^\circ$ and Rabi couplings of $(\Omega^\uparrow, \Omega^\downarrow) = 2\pi \cdot (0.52, 0.36)$ MHz. The experimental data and the amplitude-scaled theoretical expectation are overall in good agreement. Differences in theory and experiment emerge from several line-broadening effects, such as the finite size of the atoms' thermal wavepacket in radial and axial direction in the traps (Supplementary Information), which results in an averaging over a range of atom pair separations and angles within the radial ground state wavepacket size of $\sigma_{\text{rad}}^0 = 0.15 \mu\text{m}$ and the axial

thermal wavepacket size $\sqrt{2\sigma_{\text{ax}}^0 \sqrt{k_B T / \hbar \omega_{\text{ax}}}} \approx 0.86 \mu\text{m}$ for the axial trapping frequency $\omega_{\text{ax}} = 2\pi \cdot 1.7 \text{kHz}$. A second, equally important, effect is caused by the line shifts due to tweezer-to-tweezer inhomogeneities which result in an average trap depth difference of $|\Delta U| = h \cdot (10.6 \pm 1.6) \text{kHz}$. In addition, laser phase noise currently limits the dressing time due to a 20-fold increased scattering rate appearing as atom loss [43].

We additionally map out the angular dependence of the flop-flop interaction for a fixed distance of $5.6 \mu\text{m}$ and Rabi couplings of $(\Omega^\uparrow, \Omega^\downarrow) = 2\pi \cdot (0.55, 0.30) \text{MHz}$. In this measurement, we cross a singularity in the spin-spin coupling at $\theta \approx 30^\circ$ caused by a Rydberg pair state resonance. We reproduce a peaked interaction around this resonance, shown in Fig. 4d, while the broadening effects explain the weak atom loss by direct Rydberg excitation on resonance (Supplementary Information).

In the second set of measurements, we switch on both flop-flop and flip-flop interactions by setting the detunings to $(\Delta^\uparrow, \Delta^\downarrow) = 2\pi \cdot (1.4, -0.6) \text{MHz}$ and Rabi frequencies to $(\Omega^\uparrow, \Omega^\downarrow) = 2\pi \cdot (0.5, 0.36) \text{MHz}$. For the analysis of the spin interactions, we take into account different initial states prepared in the statistical loading of the traps (see Fig. 4). These configurations of interest are chosen in postselection and correspond to either a fully loaded group ($|\uparrow\uparrow\uparrow\rangle$) or groups where only two out of three tweezers at the nearest neighbor distance are filled ($|\uparrow\uparrow\circ\rangle$, $|\circ\uparrow\uparrow\rangle$, where \circ indicates an empty site). In the latter configuration, only flop-flop processes occur, while in the case of three atoms also flip-flop processes appear. Comparing the two fluorescence images before and after the dressing phase allows us to identify which interaction processes occurred. More precisely, assuming a $|\uparrow\uparrow\uparrow\rangle$ occupation at the beginning, a flop-flop interaction can produce a $|\uparrow\downarrow\downarrow\rangle$ ($|\downarrow\downarrow\uparrow\rangle$) arrangement, and flip-flop processes introduce the $|\downarrow\uparrow\downarrow\rangle$ state, after push out detected as $|\downarrow\circ\downarrow\rangle$. The pure flop-flop process results in the presence of two atoms at the nearest neighbor distance on the second image. We predict a different spatial dependence of J^{++} and J^{+-} (see Fig. 4b,c). Note that the detection method used here always requires flop-flop to be present in order to initiate the dynamics out of the fully polarized initial state.

Our data reveals the angular- and distance-dependent J_{ij}^{++} interactions for an asymmetric detuning in Fig. 4d,f. In addition, we measure a peaked occurrence of the $|\downarrow\circ\downarrow\rangle$ pattern, which we identify as the flip-flop interaction shown in Fig. 4e. This feature reflects the tunability of our system by introducing J_{ij}^{+-} interactions for a given laser detuning, atom pair distance, and angle. In addition, we probe our system such that the flip-flop interaction strength vanishes and only flop-flop interactions occur (see Fig. 4f,g). Here, we scanned the angular dependence of the interactions at a fixed distance of $5.3 \mu\text{m}$ without crossing a Rydberg pair resonance. The minimum in the signal, around 65° , is

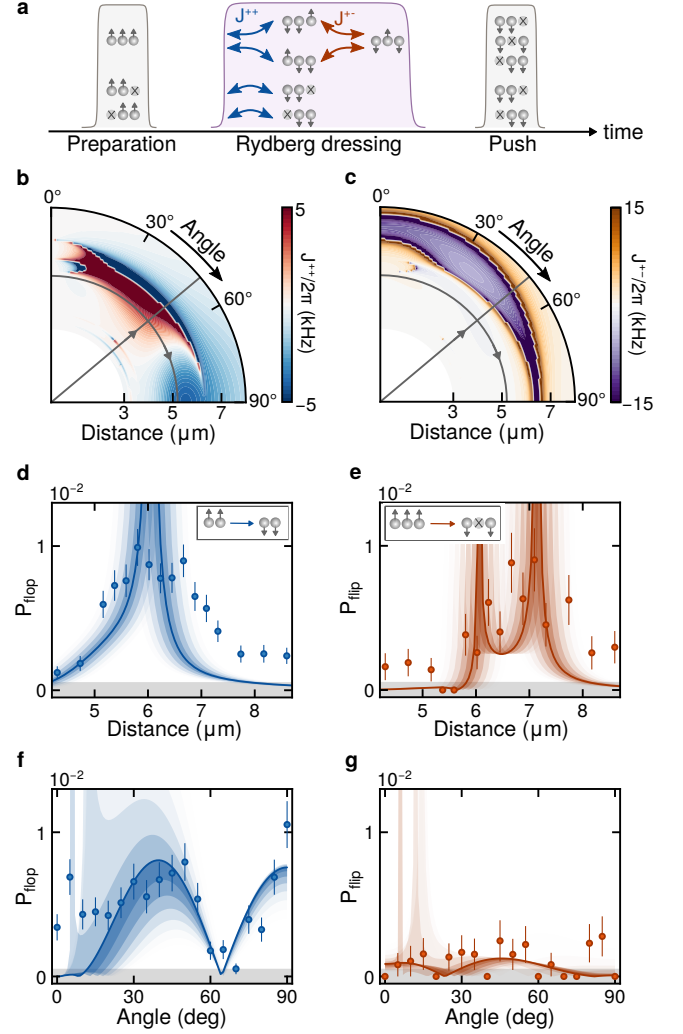


Figure 4. **Flip-Flop interactions.** **a.** Experimental sequence. We start with optically pumping all atoms in the $|\uparrow\rangle$ state. This is followed by a period of Rydberg dressing and a push out pulse, leaving only atoms in the $|\downarrow\rangle$ state. We post select two initial configurations: The atom in the center plus one additional atom or all three atoms are loaded. Depending on this configuration, flop-flop (blue arrow) and/or flip-flop processes (orange arrow) occur. **b, c.** Calculation of the distance- and angular-dependent flop-flop and flip-flop interactions. **d, e.** Distance dependence of the J^{++} and J^{+-} interactions at an angle of $\theta = 50^\circ$ (straight grey line in b, c). **f, g.** Angular dependence of the J^{++} and J^{+-} interactions at a distance of $5.3 \mu\text{m}$ (curved grey line in b, c). Shadings indicate the detection limit and the effects of the spatial extension of the atomic wavepacket analogous to figure 2; error bars denote 1 s.e.m.

caused by interference on the two-atom level. Multiple Rydberg pair states $|\Psi_\alpha^{(2)}\rangle$ with admixtures $c_\alpha^{\uparrow\uparrow} c_\alpha^{\downarrow\downarrow}$ of opposite sign contribute such that J^{++} vanishes.

In conclusion, we have demonstrated two-color Rydberg-dressing as a new technique to achieve tunable, XYZ-type short-range spin interactions in optical

tweezer arrays. Technical limitations currently prevent us from probing coherent interactions (see Supplementary Information). The two leading limitations stem from tweezer-to-tweezer line shifts due to array inhomogeneities and from laser phase noise. None of these are fundamental, in fact, other groups have reported tweezer arrays with less than 1.1% inhomogeneity [44], a factor of 10 improvement over our arrays. Laser phase noise can be filtered by optical cavities, as demonstrated for Rydberg excitation in ref. [45]. Furthermore, it is has been shown that the observed Rydberg pair state resonances can be utilized to enhance the coherence of Rydberg dressing [38]. By implementing these measures, we estimate that a maximum figure of merit, measured as the product of the peak interaction strength and the coherence time, of up to one hundred is reachable with current laser technology. This will allow one to realize a flexibly programmable analog quantum simulation platform for many-body quantum spin problems. Not only the ratio of the spin-interactions in the different channels can be controlled, but also the ratio of nearest-to next-nearest-neighbor interactions. This is rooted in

the non-monotonic spatial dependence of the interaction strength, which can also be used to design interactions in two-dimensions for the realization of a variety of frustrated geometries [33], static [39] or dynamic gauge fields [40].

Data and materials availability: The experimental and theoretical data and evaluation scripts that support the findings of this study are available on Zenodo [46].

ACKNOWLEDGMENTS

Acknowledgments: This project has received funding from the European Research Council (ERC) under Grant agreement No. 678580. We also acknowledge funding from Deutsche Forschungsgemeinschaft (GR 4741/4-1), within SPP 1929 GiRyd (GR 4741/5-1), via a Heisenberg professorship (GR 4741/3-1) and from the Alfried Krupp von Bohlen und Halbach foundation.

-
- [1] J. I. Cirac and P. Zoller, Goals and opportunities in quantum simulation, *Nature Phys.* **8**, 264 (2012).
- [2] I. M. Georgescu, S. Ashhab, and F. Nori, Quantum simulation, *Rev. Mod. Phys.* **86**, 153 (2014).
- [3] C. Gross and I. Bloch, Quantum simulations with ultracold atoms in optical lattices, *Science* **357**, 995 (2017).
- [4] M. Morgado and S. Whitlock, Quantum simulation and computing with Rydberg-interacting qubits, *AVS Quantum Sci.* **3**, 023501 (2021).
- [5] A. M. Kaufman and K. K. Ni, Quantum science with optical tweezer arrays of ultracold atoms and molecules, *Nature Phys.* **17**, 1324 (2021).
- [6] H. Bernien, S. Schwartz, A. Keesling, H. Levine, A. Omran, H. Pichler, S. Choi, A. S. Zibrov, M. Endres, M. Greiner, V. Vuletić, and M. D. Lukin, Probing many-body dynamics on a 51-Atom quantum simulator, *Nature* **551**, 579 (2017).
- [7] S. De Léséleuc, V. Lienhard, P. Scholl, D. Barredo, S. Weber, N. Lang, H. P. Büchler, T. Lahaye, and A. Browaeys, Observation of a symmetry-protected topological phase of interacting bosons with Rydberg atoms, *Science* **365**, 775 (2019).
- [8] I. S. Madjarov, A. Cooper, A. L. Shaw, J. P. Covey, V. Schkolnik, T. H. Yoon, J. R. Williams, and M. Endres, An Atomic-Array Optical Clock with Single-Atom Readout, *Phys. Rev. X* **9**, 041052 (2019).
- [9] M. A. Norcia, A. W. Young, W. J. Eckner, E. Oelker, J. Ye, and A. M. Kaufman, Seconds-scale coherence on an optical clock transition in a tweezer array, *Science* **366**, 93 (2019).
- [10] G. Semeghini, H. Levine, A. Keesling, S. Ebadi, T. T. Wang, D. Bluvstein, R. Verresen, H. Pichler, M. Kalinowski, R. Samajdar, A. Omran, S. Sachdev, A. Vishwanath, M. Greiner, V. Vuletić, and M. D. Lukin, Probing topological spin liquids on a programmable quantum simulator, *Science* **374**, 1242 (2021).
- [11] A. Byun, M. Kim, and J. Ahn, Finding the Maximum Independent Sets of Platonic Graphs Using Rydberg Atoms, *Phys. Rev. X Quantum* **3**, 030305 (2022).
- [12] D. Bluvstein, H. Levine, G. Semeghini, T. T. Wang, S. Ebadi, M. Kalinowski, A. Keesling, N. Maskara, H. Pichler, M. Greiner, V. Vuletic, and M. D. Lukin, A quantum processor based on coherent transport of entangled atom arrays, *Nature* **604**, 451 (2022).
- [13] I. S. Madjarov, J. P. Covey, A. L. Shaw, J. Choi, A. Kale, A. Cooper, H. Pichler, V. Schkolnik, J. R. Williams, and M. Endres, High-fidelity entanglement and detection of alkaline-earth Rydberg atoms, *Nature Phys.* **16**, 857 (2020).
- [14] S. Ebadi, T. T. Wang, H. Levine, A. Keesling, G. Semeghini, A. Omran, D. Bluvstein, R. Samajdar, H. Pichler, W. W. Ho, S. Choi, S. Sachdev, M. Greiner, V. Vuletić, and M. D. Lukin, Quantum phases of matter on a 256-atom programmable quantum simulator, *Nature* **595**, 227 (2021).
- [15] P. Scholl, M. Schuler, H. J. Williams, A. A. Eberharter, D. Barredo, K. N. Schymik, V. Lienhard, L. P. Henry, T. C. Lang, T. Lahaye, A. M. Läuchli, and A. Browaeys, Quantum simulation of 2D antiferromagnets with hundreds of Rydberg atoms, *Nature* **595**, 233 (2021).
- [16] D. Bluvstein, A. Omran, H. Levine, A. Keesling, G. Semeghini, S. Ebadi, T. T. Wang, A. A. Michailidis, N. Maskara, W. W. Ho, S. Choi, M. Serbyn, M. Greiner, V. Vuletić, and M. D. Lukin, Controlling quantum many-body dynamics in driven Rydberg atom arrays, *Science* **371**, 1355 (2021).
- [17] H. Weimer, M. Müller, I. Lesanovsky, P. Zoller, and H. P. Büchler, A Rydberg quantum simulator, *Nature Phys.* **6**, 382 (2010).
- [18] J. Zeiher, P. Schauß, S. Hild, T. Macrì, I. Bloch, and

- C. Gross, Microscopic Characterization of Scalable Coherent Rydberg Superatoms, *Phys. Rev. X* **5**, 031015 (2015).
- [19] D. Barredo, H. Labuhn, S. Ravets, T. Lahaye, A. Browaeys, and C. S. Adams, Coherent Excitation Transfer in a Spin Chain of Three Rydberg Atoms, *Phys. Rev. Lett.* **114**, 113002 (2015).
- [20] A. Browaeys and T. Lahaye, Many-body physics with individually controlled Rydberg atoms, *Nature Phys.* **16**, 132 (2020).
- [21] A. Signoles, T. Franz, R. Ferracini Alves, M. Gärttner, S. Whitlock, G. Zürn, and M. Weidemüller, Glassy Dynamics in a Disordered Heisenberg Quantum Spin System, *Phys. Rev. X* **11**, 11011 (2021).
- [22] P. Scholl, H. J. Williams, G. Bornet, F. Wallner, D. Barredo, T. Lahaye, A. Browaeys, L. Henriët, A. Signoles, C. Hainaut, T. Franz, S. Geier, A. Tebben, A. Salzinger, G. Zürn, and M. Weidemüller, Microwave-engineering of programmable XXZ Hamiltonians in arrays of Rydberg atoms, *Phys. Rev. X Quantum* **3**, 020303 (2022).
- [23] T. Keating, R. L. Cook, A. M. Hankin, Y.-Y. Jau, G. W. Biedermann, and I. H. Deutsch, Robust quantum logic in neutral atoms via adiabatic Rydberg dressing, *Phys. Rev. A* **91**, 012337 (2015).
- [24] Y.-Y. Jau, A. M. Hankin, T. Keating, I. H. Deutsch, and G. W. Biedermann, Entangling atomic spins with a rydberg-dressed spin-flip blockade, *Nature Physics* **12**, 71 (2016).
- [25] L. I. R. Gil, R. Mukherjee, E. M. Bridge, M. P. A. Jones, and T. Pohl, Spin Squeezing in a Rydberg Lattice Clock, *Phys. Rev. Lett.* **112**, 103601 (2014).
- [26] J. Zeiher, R. van Bijnen, P. Schauß, S. Hild, J.-Y. Choi, T. Pohl, I. Bloch, and C. Gross, Many-body interferometry of a Rydberg-dressed spin lattice, *Nature Phys.* **12**, 1095 (2016).
- [27] J. Zeiher, J.-y. Choi, A. Rubio-Abadal, T. Pohl, R. van Bijnen, I. Bloch, and C. Gross, Coherent Many-Body Spin Dynamics in a Long-Range Interacting Ising Chain, *Phys. Rev. X* **7**, 41063 (2017).
- [28] A. Arias, G. Lochead, T. M. Wintermantel, S. Helmrich, and S. Whitlock, Realization of a Rydberg-Dressed Ramsey Interferometer and Electrometer, *Phys. Rev. Lett.* **122**, 053601 (2019).
- [29] E. Guardado-Sanchez, B. M. Spar, P. Schauss, R. Belyan-sky, J. T. Young, P. Bienias, A. V. Gorshkov, T. Iadecola, and W. S. Bakr, Quench Dynamics of a Fermi Gas with Strong Nonlocal Interactions, *Phys. Rev. X* **11**, 21036 (2021).
- [30] V. Borish, O. Marković, J. A. Hines, S. V. Rajagopal, and M. Schleier-Smith, Transverse-Field Ising Dynamics in a Rydberg-Dressed Atomic Gas, *Phys. Rev. Lett.* **124**, 063601 (2020).
- [31] S. Hollerith, K. Srakaew, D. Wei, A. Rubio-Abadal, D. Adler, P. Weckesser, A. Kruckenhauser, V. Walther, R. Van Bijnen, J. Rui, C. Gross, I. Bloch, and J. Zeiher, Realizing distance-selective interactions in a Rydberg-dressed atom array, *Phys. Rev. Lett.* **128**, 113602 (2021).
- [32] S. Weber, C. Tresp, H. Menke, A. Urvoy, O. Firstenberg, H. P. Büchler, and S. Hofferberth, Calculation of Rydberg interaction potentials, *J. Phys. B: At. Mol. Opt. Phys.* **50**, 133001 (2017).
- [33] A. W. Glaetzle, M. Dalmonte, R. Nath, C. Gross, I. Bloch, and P. Zoller, Designing Frustrated Quantum Magnets with Laser-Dressed Rydberg Atoms, *Phys. Rev. Lett.* **114**, 173002 (2015).
- [34] P. Schauß, J. Zeiher, T. Fukuhara, S. Hild, M. Cheneau, T. Macrì, T. Pohl, I. Bloch, and C. Gross, Crystallization in Ising quantum magnets, *Science* **347**, 1455 (2015).
- [35] V. Lienhard, S. De Léséleuc, D. Barredo, T. Lahaye, A. Browaeys, M. Schuler, L. P. Henry, and A. M. Läuchli, Observing the Space- and Time-Dependent Growth of Correlations in Dynamically Tuned Synthetic Ising Models with Antiferromagnetic Interactions, *Phys. Rev. X* **8**, 1 (2018).
- [36] K. Kim, M. S. Chang, S. Korenblit, R. Islam, E. E. Edwards, J. K. Freericks, G. D. Lin, L. M. Duan, and C. Monroe, Quantum simulation of frustrated Ising spins with trapped ions, *Nature* **465**, 590 (2010).
- [37] A. Periwal, E. S. Cooper, P. Kunkel, J. F. Wienand, E. J. Davis, and M. Schleier-Smith, Programmable interactions and emergent geometry in an array of atom clouds, *Nature* **600**, 630 (2021).
- [38] R. M. W. Van Bijnen and T. Pohl, Quantum Magnetism and Topological Ordering via Rydberg Dressing near Förster Resonances, *Phys. Rev. Lett.* **114**, 243002 (2015).
- [39] X. Wu, F. Yang, S. Yang, K. Mølmer, T. Pohl, M. K. Tey, and L. You, Manipulating synthetic gauge fluxes via multicolor dressing of Rydberg-atom arrays, *Phys. Rev. Research* **4**, L032046 (2022).
- [40] P. S. Tarabunga, F. M. Surace, R. Andreoni, A. Angelone, and M. Dalmonte, Gauge-theoretic origin of Rydberg quantum spin liquids, arxiv:2205.13000 (2022).
- [41] D. Sels and E. Demler, Quantum generative model for sampling many-body spectral functions, *Phys. Rev. B* **103**, 14301 (2021).
- [42] N. Lorenz, L. Festa, L.-M. Steinert, and C. Gross, Raman sideband cooling in optical tweezer arrays for Rydberg dressing, *SciPost Phys.* **10**, 52 (2021).
- [43] L. Festa, N. Lorenz, L.-M. Steinert, Z. Chen, P. Osterholz, R. Eberhard, and C. Gross, Blackbody-radiation-induced facilitated excitation of Rydberg atoms in optical tweezers, *Phys. Rev. A* **105**, 013109 (2022).
- [44] D. Kim, A. Keesling, A. Omran, H. Levine, H. Bernien, M. Greiner, M. D. Lukin, and D. R. Englund, Large-Scale Uniform Optical Focus Array Generation with a Phase Spatial Light Modulator, *Optics Letters* **44**, 3178 (2019).
- [45] H. Levine, A. Keesling, A. Omran, H. Bernien, S. Schwartz, A. S. Zibrov, M. Endres, M. Greiner, V. Vuletić, and M. D. Lukin, High-Fidelity Control and Entanglement of Rydberg-Atom Qubits, *Physical Review Letters* **121**, 123603 (2018).
- [46] L.-M. Steinert, P. Osterholz, R. Eberhard, L. Festa, N. Lorenz, Z. Chen, A. Trautmann, and C. Gross, Spatially programmable spin interactions in neutral atom arrays, Zenodo 10.5281/zenodo.6906497 (2022).
- [47] N. R. Hutzler, L. R. Liu, Y. Yu, and K.-K. Ni, Eliminating light shifts for single atom trapping, *New Journal of Physics* **19**, 023007 (2017).
- [48] A. Urvoy, F. Ripka, I. Lesanovsky, D. Booth, J. P. Shafer, T. Pfau, and R. Löw, Strongly correlated growth of rydberg aggregates in a vapor cell, *Physical Review Letters* **114**, 203002 (2015).

SUPPLEMENTARY INFORMATION

This supplementary information document provides information about the experimental sequence and laser setup, a detailed derivation of the interactions, and a discussion of our experimental limitations.

I. EXPERIMENTAL SEQUENCE

The optical tweezers are generated using a commercial 1064 nm laser aligned onto a liquid crystal spatial light modulator, which imprints a phase pattern onto the beam. An in-vacuum mounted objective (NA = 0.6) focuses the linearly-polarized beam, obtaining a tweezer array with controlled geometry, of which each trap has a waist of $0.9 \mu\text{m}$. We load ^{39}K atoms into the traps by alternating trapping and cooling light with a frequency of 1.4 MHz [47], one order of magnitude faster than the radial trapping frequency of $\omega_r = 2\pi \cdot 158 \text{ kHz}$ ($\omega_z = 2\pi \cdot 25 \text{ kHz}$). On average, 50% of the traps are filled with a single atom [42, 43], and the experimental cycle rate is 1 Hz.

After a first fluorescence image probing the tweezer filling, we optically pump and prepare the atoms in the $|\uparrow\rangle = |4S_{1/2} F=2, m_F=-2\rangle$ state with σ^- -polarized pumping and repumping light on the D1-line. To

quantify the state preparation efficiency, we start by preparing all the atoms in the $|\uparrow\rangle$ state. We then switch on the optical pumping light without the repump light and compare the results for two different polarizations. If the light can only drive σ^- transitions, the atoms remain in the $|\uparrow\rangle$ state, which is dark under this illumination on the D1 line. Scanning the pulse duration of the pumping light, we fit a $1/e$ optical depumping time $\tau_{\text{DP}} = 35.93 \pm 2.54 \text{ ms}$. In contrast, if the polarization is changed such that the light drives σ^+ or π transitions, the atoms are depumped to $F=1$. In the latter case, we measure a $1/e$ optical depumping time $\tau_{\text{OP}} = 0.20 \pm 0.02 \text{ ms}$. From this we extract the state preparation efficiency in the $|\uparrow\rangle$ state to be $P(F=2, m_F=-2) = 1 - \tau_{\text{OP}}/\tau_{\text{DP}} = 99.44 \pm 0.08 \%$.

We then apply Raman sideband cooling (RSC) [42], which enables us to lower the trap depth to a minimum of $h \cdot 80 \text{ kHz}$ before gravity opens the trap. At these low intensities, the light shift induced inhomogeneities of the Rydberg excitation lines are reduced to a few kHz (see section IV B). We continue with a $50 \mu\text{s}$ long pulse of both Rydberg dressing lasers (details see section II). The magnetic field strength of $B = 1 \text{ G}$ leads to a Zeeman splitting of the Rydberg states $E_z = h \cdot 1.98 \text{ MHz}$.

The Rydberg excitation beams couple the following ground states

$$\begin{aligned} |\uparrow\rangle &= |4S_{1/2}\rangle |F=2, m_F=-2\rangle = |4S_{1/2}\rangle |m_j=-1/2\rangle |m_I=-3/2\rangle \\ |\downarrow\rangle &= |4S_{1/2}\rangle |F=1, m_F=-1\rangle = |4S_{1/2}\rangle (|m_j=-1/2\rangle |m_I=-1/2\rangle - \sqrt{3}|m_j=1/2\rangle |m_I=-3/2\rangle)/2 \end{aligned} \quad (\text{S.1})$$

to the Rydberg states $|r_\uparrow\rangle = |62P_{3/2}, m_j=-3/2\rangle$ and $|r_\downarrow\rangle = |62P_{3/2}, m_j=-1/2\rangle$ respectively.

After the Rydberg laser pulse, we remove all remaining atoms in the $F=2$ manifold with a resonant laser pulse on the $|F=2, m_F=-2\rangle$ to $|F'=3, m'_F=-3\rangle$ cycling transition of the D2-line. We detect the remaining atoms in the $|\downarrow\rangle$ state with a second fluorescence image. Comparing both fluorescence images allows us to deduce the spin interactions based on spin flips and their correlations.

II. RYDBERG LASER SETUP

The Rydberg dressing laser setup consists of a home-built ECDL laser at 1143.5 nm, which is amplified to 8 W via a commercial Raman fiber amplifier and then frequency-quadrupled in two consecutive, homebuilt cavity-enhanced doubling stages. This results in an output power of 1 W at 286 nm. This UV beam is then split into two paths with acousto-optical modulators (AOM) with frequencies of $\pm 230 \text{ MHz}$, which we use for inten-

sity stabilization and bridging the hyperfine ground state splitting. The beams are then overlapped and focused onto the atoms, with a horizontal waist of $40 \mu\text{m}$ and a vertical waist of $10 \mu\text{m}$. The Rydberg excitation beams propagate parallel to the magnetic field and drive σ^- transitions.

The lifetime of the dressed ground states is proportional to the Rydberg state probability. For our parameters and assuming a phase-noise-free laser, we expect a dressed (black-body radiation limited) lifetime of $\tau_{\text{dr}} = 1.7 \text{ ms}$. In contrast, the experimentally observed lifetime is reduced to $70 \mu\text{s}$ (for $\Delta_\downarrow = -2\pi \cdot 0.6 \text{ MHz}$ and $\Omega_\downarrow = 2\pi \cdot 0.4 \text{ MHz}$) due to laser noise [43]. Atom loss due to excitation to Rydberg pair resonances is weak, as shown in Fig. S1. Here, the data has been postselected to only nearest neighbor tweezer pairs initially loaded. In the measurement, we did not apply a push out pulse, to realize spin-insensitive imaging. All Rabi frequencies have been measured before the respective set of measurement runs by driving Rabi oscillations without trapping light. The typical uncertainty of the Rabi frequency fits is 0.01 MHz.

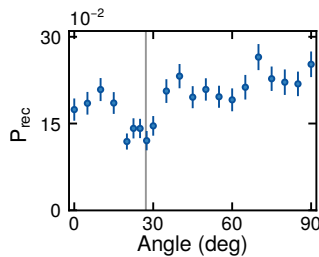


Figure S1. **Atom loss on Rydberg pair resonance.** Measurement settings are the same as in Fig. 2d in the main text. The gray vertical line marks the predicted position of the pair state resonance. The data shown has been analyzed on a postselected dataset which includes only tweezers with at two nearest neighbor atoms loaded $|\uparrow\uparrow\rangle$ ($|\circ\uparrow\uparrow\rangle$). No push out pulse was applied at the end of the sequence to realize a spin-insensitive measurement. The atom loss on resonance is observable but weak for our settings.

III. DERIVATION OF THE EFFECTIVE INTERACTIONS

The effective spin-spin interactions between dressed ground states arise adiabatically by the elimination of the Rydberg levels in the two-atom Hamiltonian $\hat{H} = \hat{H}_{\text{las}} + \hat{H}_{\text{int}}$. The ground states are laser coupled to the Rydberg states by the laser coupling Hamiltonian

$$\begin{aligned} \hat{H}_{\text{las}}/\hbar = & \sum_{i=1}^2 [\Omega^\uparrow (|\uparrow\rangle\langle r^\uparrow|_i + |r^\uparrow\rangle\langle\uparrow|_i)/2 + \Omega^\downarrow (|\downarrow\rangle\langle r^\downarrow|_i \\ & - |r^\downarrow\rangle\langle\downarrow|_i)/2 + \Delta^\uparrow |r^\uparrow\rangle\langle r^\uparrow|_i - \Delta^\downarrow |r^\downarrow\rangle\langle r^\downarrow|_i] \end{aligned} \quad (\text{S.2})$$

The Rabi frequency Ω^σ determines the coupling strength between a ground state $|\sigma\rangle_i$ and a Rydberg state $|r^\sigma\rangle_i$ of one atom i , with $\sigma \in \{\uparrow, \downarrow\}$. For the chosen laser polarizations and states, the dipole matrix elements between $|\uparrow\rangle_i$ and $|r^\downarrow\rangle_i$ and vice versa vanish, such that single-atom Raman transitions are absent. The magnetic field dependent single atom detunings are described by Δ^σ .

The pair interaction Hamiltonian \hat{H}_{int} arises from the dipolar interactions among the Rydberg states. We use the ‘‘pairinteraction’’ software package to diagonalize the interaction Hamiltonian [32] and to obtain the pair-separation d and -angle θ dependent eigenstates $|\Psi_\alpha^{(2)}\rangle$ with eigenenergies $E_\alpha(d, \theta)$. The eigenstates can be developed in asymptotic pair states $|r^m r^n\rangle$ as $|\Psi_\alpha^{(2)}\rangle = \sum_{nm} c_\alpha^{mn}(d, \theta) |r^m r^n\rangle$ with the distance- and angle dependent admixture $c_\alpha^{mn}(d, \theta) = \langle \Psi_\alpha^{(2)} | r^m r^n \rangle$. To improve the readability, we suppress the explicit d, θ -dependency in the rest of the text.

The dipolar interactions between any pair of Rydberg states $|r^m r^n\rangle$ can be written in the pair basis $\{|r^m r^m\rangle, |r^m r^n\rangle, |r^n r^m\rangle, |r^n r^n\rangle\}$ in the form

$$\hat{H}_{\text{int}} = \begin{pmatrix} V^{mm,mm} & 0 & 0 & V^{mm,nn} \\ 0 & V^{mn,mn} & V^{mn,nm} & 0 \\ 0 & V^{nm,mn} & V^{nm,nm} & 0 \\ V^{nn,mm} & 0 & 0 & V^{nn,nn} \end{pmatrix}. \quad (\text{S.3})$$

When adiabatically eliminating the Rydberg states (equivalent to 4-th order perturbation theory, c.f. ref. [33]), this form of the interactions is transferred to the dressed ground states and the effective Hamiltonian \hat{H}_{eff} reads in the $\{|\uparrow\uparrow\rangle, |\uparrow\downarrow\rangle, |\downarrow\uparrow\rangle, |\downarrow\downarrow\rangle\}$ basis:

$$\hat{H}_{\text{eff}} = \begin{pmatrix} W^{\uparrow\uparrow,\uparrow\uparrow} & 0 & 0 & W^{\uparrow\uparrow,\downarrow\downarrow} \\ 0 & W^{\uparrow\downarrow,\uparrow\downarrow} & W^{\uparrow\downarrow,\downarrow\uparrow} & 0 \\ 0 & W^{\downarrow\uparrow,\uparrow\downarrow} & W^{\downarrow\uparrow,\downarrow\uparrow} & 0 \\ W^{\downarrow\downarrow,\uparrow\uparrow} & 0 & 0 & W^{\downarrow\downarrow,\downarrow\downarrow} \end{pmatrix}. \quad (\text{S.4})$$

In the following, we develop an intuitive picture for deriving the different entries of this effective interaction matrix. The general idea is a step-wise elimination of the Rydberg levels, starting with singly excited states to obtain a Λ -system. In the second step, we also eliminate the doubly excited states to arrive at an effective Hamiltonian for the dressed ground states. This procedure is illustrated in Fig. S2. Here, we assume that there are only four relevant (i.e. near-resonantly) laser coupled asymptotic pair states, the states $\{|r^\uparrow r^\uparrow\rangle, |r^\uparrow r^\downarrow\rangle, |r^\downarrow r^\uparrow\rangle, |r^\downarrow r^\downarrow\rangle\}$.

A. The diagonal coupling terms

For the derivation of $W^{\sigma\sigma,\sigma\sigma}$, we start with adiabatic elimination of the single excited state $|+\sigma\rangle = (|\sigma r^\sigma\rangle + |r^\sigma\sigma\rangle)/\sqrt{2}$. For large atom distances, we obtain the effective two-photon Rabi couplings $\Omega^{\sigma\sigma} = (\Omega^\sigma)^2/2\Delta^\sigma$. At short distances, the pair potentials in the m_j -subspace of the $62P_{3/2}$ manifold interact with each other via dipole-quadrupole interaction, which leads to avoided crossings and mixing of Rydberg states [48]. The corresponding admixture $c_\alpha^{\sigma\sigma} = \langle \Psi_\alpha^{(2)} | r^\sigma r^\sigma \rangle$ of $|r^\sigma r^\sigma\rangle$ in close-by interacting pairstates $|\Psi_\alpha^{(2)}\rangle$ reduces the effective Rabi frequencies to $\Omega_\alpha^{\sigma\sigma} = \Omega_{\text{eff}}^{\sigma\sigma} \cdot c_\alpha^{\sigma\sigma}$. We then adiabatically eliminate the Rydberg pairstates and subtract the asymptotic value of $W^{\sigma\sigma,\sigma\sigma}$ for $d = \infty$ to eliminate a constant offset.

$$W^{\sigma\sigma,\sigma\sigma} = \frac{(\Omega^\sigma)^4}{4(\Delta^\sigma)^2} \sum_\alpha \left(\frac{(c_\alpha^{\sigma\sigma})^2}{\Delta_\alpha^{(2)}} - \frac{1}{2\Delta^\sigma} \right), \quad (\text{S.5})$$

with the Rydberg pair state detuning $\Delta_\alpha^{(2)} = 2\Delta^\sigma - E_\alpha$.

The derivation of the $W^{\sigma\bar{\sigma},\sigma\bar{\sigma}}$ (with $\sigma \neq \bar{\sigma}$) is similar: As there are two excitation paths from $|\sigma\bar{\sigma}\rangle$ to $|\Psi_\alpha^{(2)}\rangle$, the reduced two-photon coupling is

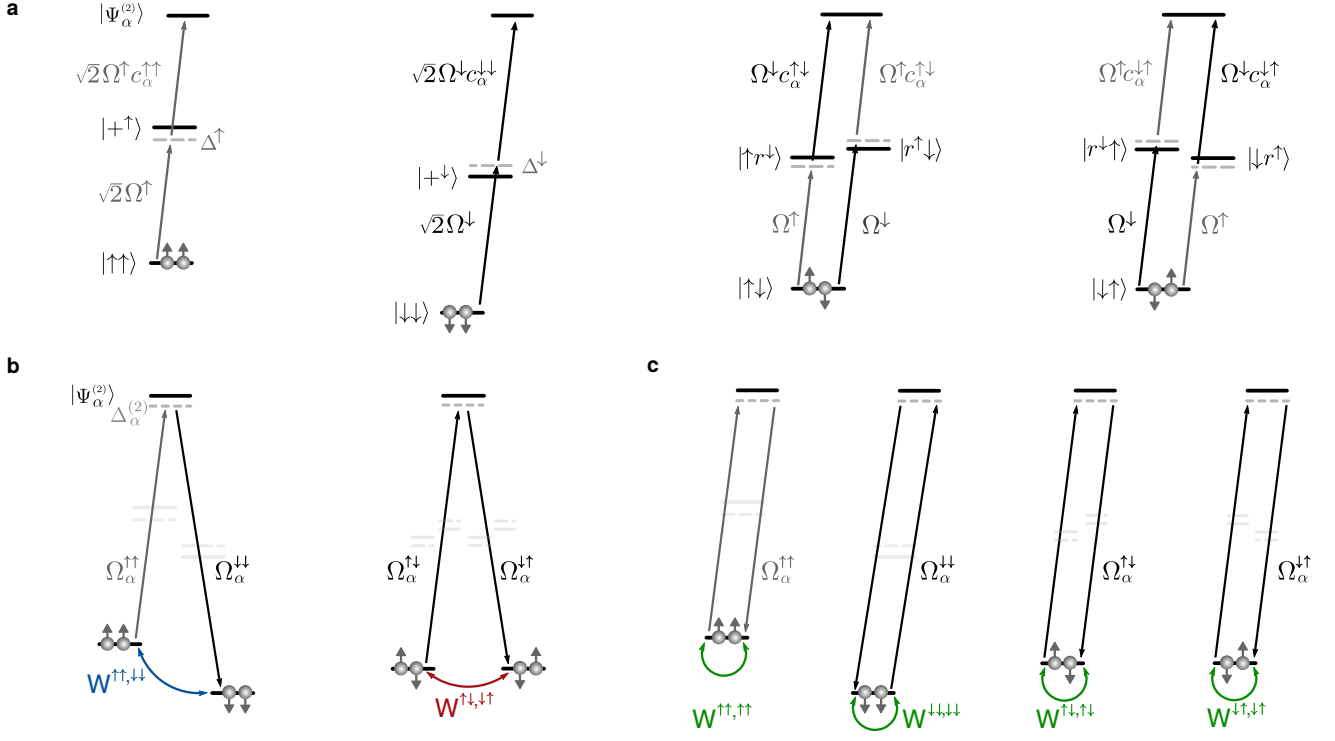


Figure S2. **Stepwise adiabatic elimination.** **a.** Elimination of singly excited Rydberg states. We show the level schemes corresponding to the coupling of different ground state spin-pairs to the Rydberg manifold. The singly excited states are adiabatically eliminated to obtain an effective pair state coupling $\Omega_{\alpha}^{\sigma\sigma'}$ to the eigenstates of the dipolar interaction Hamiltonian $|\Psi_{\alpha}^{(2)}\rangle$. **b.** Elimination of doubly excited states. The result of the first elimination step is an effective Λ -system, in which we eliminate the doubly excited states $|\Psi_{\alpha}^{(2)}\rangle$ to obtain effective ground state coupling (for unequal initial and final states), or a light shift (for equal initial and final states).

$\Omega_{\alpha}^{\sigma\bar{\sigma}} = (\Omega^{\sigma}\Omega^{\bar{\sigma}}/4\Delta^{\sigma} + \Omega^{\sigma}\Omega^{\bar{\sigma}}/4\Delta^{\bar{\sigma}}) \cdot c_{\alpha}^{\sigma\bar{\sigma}}$. Again we adiabatically eliminate $|\Psi_{\alpha}^{(2)}\rangle$ and remove a constant offset by subtracting the $d = \infty$ asymptotic value to obtain:

$$W^{\sigma\bar{\sigma},\sigma\bar{\sigma}} = \left(\frac{1}{(\Delta^{\sigma})^2} + \frac{1}{(\Delta^{\bar{\sigma}})^2} + \frac{1}{\Delta^{\sigma}\Delta^{\bar{\sigma}}} \right) \frac{(\Omega^{\sigma})^2(\Omega^{\bar{\sigma}})^2}{16} \cdot \sum_{\alpha} \left(\frac{(c_{\alpha}^{\sigma\bar{\sigma}})^2}{\Delta_{\alpha}^{(2)}} - \frac{1}{2\Delta^{\sigma}} - \frac{1}{2\Delta^{\bar{\sigma}}} \right) \quad (\text{S.6})$$

B. The flop-flop off-diagonal terms

The flop-flop coupling terms $W^{\sigma\sigma,\bar{\sigma}\bar{\sigma}}$ are derived analogously. The effective Rabi frequencies for the flop-flop interactions are $\Omega_{\alpha}^{\sigma\sigma} = \Omega_{\text{eff}}^{\sigma\sigma} \cdot c_{\alpha}^{\sigma\sigma}$. Via adiabatic elimination of the Rydberg pair states, we obtain the flop-flop coupling term. For the off-diagonal terms, offsets at $d = \infty$ are absent since there are two different asymptotic pair state overlaps involved, and one of them must vanish asymptotically. We obtain:

$$W^{\sigma\sigma,\bar{\sigma}\bar{\sigma}} = \sum_{\alpha} \frac{\Omega_{\alpha}^{\sigma\sigma}\Omega_{\alpha}^{\bar{\sigma}\bar{\sigma}}}{\Delta_{\alpha}^{(2)}} = \sum_{\alpha} \frac{(\Omega^{\sigma}\Omega^{\bar{\sigma}})^2}{4\Delta^{\sigma}\Delta^{\bar{\sigma}}} \cdot \frac{c_{\alpha}^{\sigma\sigma}c_{\alpha}^{\bar{\sigma}\bar{\sigma}}}{\Delta_{\alpha}^{(2)}} \quad (\text{S.7})$$

C. The flip-flop off-diagonal terms

For the flip-flop term $W^{\sigma\bar{\sigma},\bar{\sigma}\sigma}$ we adiabatically eliminate the single excited states $|r^{\sigma}\bar{\sigma}\rangle$ and obtain the reduced two-photon Rabi couplings $\Omega_{\alpha}^{\sigma\bar{\sigma}} = (\Omega^{\sigma}\Omega^{\bar{\sigma}}/4\Delta^{\sigma} + \Omega^{\sigma}\Omega^{\bar{\sigma}}/4\Delta^{\bar{\sigma}}) \cdot c_{\alpha}^{\sigma\bar{\sigma}}$. Here, the destructive interference of the two excitation paths for equal magnitude but opposite sign detunings becomes apparent. Via adiabatic elimination of the Rydberg manifold, we obtain the flip-flop coupling term:

$$W^{\sigma\bar{\sigma},\bar{\sigma}\sigma} = \sum_{\alpha} \frac{\Omega_{\alpha}^{\sigma\bar{\sigma}}\Omega_{\alpha}^{\bar{\sigma}\sigma}}{\Delta_{\alpha}^{(2)}} = \sum_{\alpha} \left(\frac{\Omega^{\sigma}\Omega^{\bar{\sigma}}}{4\Delta^{\sigma}} + \frac{\Omega^{\bar{\sigma}}\Omega^{\sigma}}{4\Delta^{\bar{\sigma}}} \right)^2 \frac{c_{\alpha}^{\sigma\bar{\sigma}}c_{\alpha}^{\bar{\sigma}\sigma}}{\Delta_{\alpha}^{(2)}} \quad (\text{S.8})$$

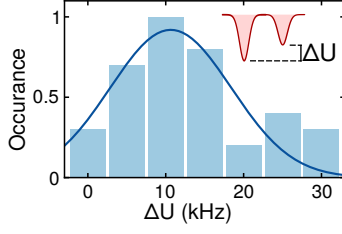


Figure S3. **Tweezer inhomogeneities.** Distribution of the trap depth difference $|\Delta U|$ for two tweezers at the nearest neighbor distance and for the minimum trap depth of $h \cdot 80$ kHz. The Gaussian fit (solid line) reveals an average trap depth difference of $|\overline{\Delta U}| = h \cdot (10.6 \pm 1.6)$ kHz. For our tweezers generated with 1064 nm light, the magnitude of the ponderomotive potential for the Rydberg states approximately equals the trap depth for the ground states but is of the opposite sign. Hence, the difference in the line shifts of the ground state-Rydberg transition for nearest-neighbor pairs is about $2|\Delta U|$.

D. Formulation of an effective spin Hamiltonian

The XYZ-Hamiltonian written in terms of Pauli matrices $\sigma^x, \sigma^y, \sigma^z$ reads

$$\hat{H}_{\text{XYZ}} = \hbar \sum_{ij} [J_{ij}^x \sigma_i^x \sigma_j^x + J_{ij}^y \sigma_i^y \sigma_j^y + J_{ij}^z \sigma_i^z \sigma_j^z], \quad (\text{S.9})$$

or alternatively in raising/lowering form

$$\begin{aligned} \hat{H}_{\text{XYZ}} = \hbar \sum_{ij} [& J_{ij}^{x+} (\sigma_i^+ \sigma_j^- + \sigma_i^- \sigma_j^+) \\ & + J_{ij}^{y+} (\sigma_i^+ \sigma_j^+ + \sigma_i^- \sigma_j^-) + J_{ij}^z \sigma_i^z \sigma_j^z], \end{aligned} \quad (\text{S.10})$$

with $\sigma_i^x = (\sigma_i^- + \sigma_i^+)$, $\sigma_i^y = i(\sigma_i^- - \sigma_i^+)$, the flop-flop coupling $J_{ij}^{x+} = (J_{ij}^x - J_{ij}^y)$ and the flip-flop coupling $J_{ij}^{+-} = (J_{ij}^x + J_{ij}^y)$.

By expanding Eq. S.10 in the ground state pair basis and comparing to Eq. S.4 one identifies

$$\begin{aligned} J_{ij}^z &= W^{\uparrow\uparrow, \uparrow\uparrow}(d_{ij}, \theta_{ij}) + W^{\downarrow\downarrow, \downarrow\downarrow}(d_{ij}, \theta_{ij}) \\ &\quad - 2W^{\uparrow\downarrow, \uparrow\downarrow}(d_{ij}, \theta_{ij}) \\ J_{ij}^{+-} &= 2W^{\uparrow\downarrow, \downarrow\uparrow}(d_{ij}, \theta_{ij}) \\ J_{ij}^{++} &= 2W^{\uparrow\uparrow, \downarrow\downarrow}(d_{ij}, \theta_{ij}) \end{aligned} \quad (\text{S.11})$$

where we used $W^{\uparrow\downarrow, \uparrow\downarrow} = W^{\downarrow\uparrow, \downarrow\uparrow}$, $W^{\downarrow\uparrow, \uparrow\downarrow} = W^{\uparrow\downarrow, \downarrow\uparrow}$, and $W^{\uparrow\uparrow, \downarrow\downarrow} = W^{\downarrow\downarrow, \uparrow\uparrow}$. For clarity, we also restored the pair-separation and -angle dependence here.

IV. EXPERIMENTAL LIMITATIONS

In our setup, laser noise and inhomogeneous line shifts due to the trapping laser are the main limitations preventing us from probing coherent interactions. In the

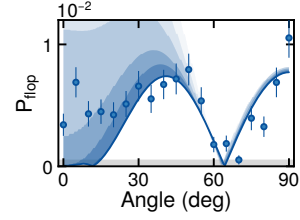


Figure S4. **Influence of the out-of-plane position fluctuations.** Data points are the same as in Fig. 3f in the main text. The shading represents the effect of the axial motion of the atoms in traps.

following, we discuss these limitations and their consequences.

A. Laser noise

Phase noise of our Rydberg excitation laser results in an incoherently enhanced population of the Rydberg states. The Rydberg population is determined by $\beta^2 = \Omega^2/4\Delta^2$ for negligible noise, resulting in an excitation rate of $\beta^2\gamma_r$. Here, γ_r^{-1} is the Rydberg-state lifetime. In our experiment, we measure an about 20-fold increased scattering rate by observing the trap loss [43].

B. Inhomogeneity of trap depths

To determine the depth of the tweezers, we measure the AC Stark shift on the D1-line by spectroscopy. We first prepare the atoms in the $|F = 2, m_F = 2\rangle$ state and set the magnetic field perpendicular to the optical beams such that we probe different polarizations. On resonance, the atoms are pumped to the $F = 1$ hyperfine manifold. We then adiabatically rotate the magnetic field parallel to the direction of the laser beam and remove all atoms in the $F = 2$ hyperfine manifold with light resonant to the $|F = 2, m_F = 2\rangle$ to $|F' = 3, m_{F'} = 3\rangle$ cycling transition of the D2-line. We measure the light shift at an average trap depth of 200 μK and scale the results to the minimal depth used for experiments described in the main text. In Fig. S3 we show the nearest-neighbor tweezer trap depth difference $|\Delta U|$ of a 3x14 tweezer array.

C. In-trap wavepacket size

Tweezer inhomogeneities force us to work at a minimal trap depth of $h \cdot 80$ kHz. This results in a radial (axial) trapping frequency of $\omega_{\text{rad}} = 2\pi \cdot 11$ kHz ($\omega_{\text{ax}} = 2\pi \cdot 1.7$ kHz) with corresponding radial (axial) ground state wavepacket sizes of $\sigma_{\text{rad}}^0 = \sqrt{\hbar/(m\omega_{\text{rad}})} = 0.15 \mu\text{m}$ ($\sigma_{\text{ax}}^0 = 0.39 \mu\text{m}$).

The temperature of our Raman cooled atoms corresponds to $k_B T = h \cdot 4.2$ kHz as measured in ref. [42]. Since

the temperature is below the trapping frequency in radial direction we use the ground state wavepacket size to estimate the radial pair-distance fluctuations $\sigma_{\text{rad}} \approx \sqrt{2}\sigma_{\text{rad}}^0$. The factor $\sqrt{2}$ takes the independent motion of the two atoms into account.

The impact of the axial (out-of-plane) wave packet sizes is much weaker and we neglect its effect in the main text. Nevertheless, it explains the comparably strong

flop-flop interactions for small angles for the measurement shown in Fig. 3f of the main text. In Fig. S4 we show the effect of a thermal wavepacket of size $\sqrt{2}\sigma_{\text{ax}}^0\sqrt{k_B T/\hbar\omega_{\text{ax}}} \approx 0.86 \mu\text{m}$ on the flop-flop interactions. We use the large temperature limit for the estimation of the position fluctuations here since $k_B T > \hbar\omega_{\text{ax}}$. The out-of-plane fluctuations result in an averaging over a range of angles, removing the zero in the interactions at a mean angle of $\theta = 0^\circ$.